

# The Surface of 2003 EL<sub>61</sub> in the Near Infrared

Chadwick A. Trujillo

*Gemini Observatory, Northern Operations Center, 670 N. A'ohoku Place, Hilo, Hawaii  
96720*

[trujillo@gemini.edu](mailto:trujillo@gemini.edu)

and

Michael E. Brown

*California Institute of Technology, Division of Geological and Planetary Sciences, MS  
150-21, Pasadena, California 91125*

[mbrown@caltech.edu](mailto:mbrown@caltech.edu)

and

Kristina M. Barkume

*California Institute of Technology, Division of Geological and Planetary Sciences, MS  
150-21, Pasadena, California 91125*

[barkume@gps.caltech.edu](mailto:barkume@gps.caltech.edu)

and

Emily L. Schaller

*California Institute of Technology, Division of Geological and Planetary Sciences, MS  
150-21, Pasadena, California 91125*

[emily@gps.caltech.edu](mailto:emily@gps.caltech.edu)

and

David L. Rabinowitz

*Yale Center for Astronomy and Astrophysics, Physics Department, Yale University, P.O.  
Box 208121, New Haven, Connecticut 06520-8121*

[david.rabinowitz@yale.edu](mailto:david.rabinowitz@yale.edu)

Submitted to the Astrophysical Journal Jan 20, 2006

## ABSTRACT

We report the detection of crystalline water ice on the surface of 2003 EL<sub>61</sub>. Reflectance spectra were collected from Gemini North telescope from 1.0 to 2.4  $\mu\text{m}$  wavelength range, and from the Keck telescope across the 1.4 to 2.4  $\mu\text{m}$  wavelength range. The signature of crystalline water ice is clear and obvious in all data collected. Like the surface of many outer solar system bodies, the surface of 2003 EL<sub>61</sub> is rich in crystalline water ice, which is energetically less favored than amorphous water ice at cold temperatures, suggesting resurfacing processes may be taking place. The near infrared color of the object is much bluer than a pure water ice model. Adding a near infrared blue component such as hydrogen cyanide or phyllosilicate clays improves the fit considerably, with hydrogen cyanide providing the greatest improvement. The addition of hydrated tholins and bitumens also improves the fit but is inconsistent with the neutral  $V - J$  reflectance of 2003 EL<sub>61</sub>. A small decrease in reflectance beyond 2.3  $\mu\text{m}$  may be attributable to cyanide salts. Overall, the reflected light from 2003 EL<sub>61</sub> is best fit by a model of 2/3 to 4/5 pure crystalline water ice and 1/3 to 1/5 near infrared blue component such as hydrogen cyanide or kaolinite. The surface of 2003 EL<sub>61</sub> is unlikely to be covered by significant amounts of dark material such as carbon black, as our pure ice models reproduce published albedo estimates derived from the spin state of 2003 EL<sub>61</sub>.

*Subject headings:* comets: general — Kuiper Belt — solar system: formation

## 1. Introduction

The Kuiper belt objects (KBOs) have been known for a decade to have the most diverse surfaces of any minor planet population in terms of global color at visible wavelengths (Luu & Jewitt 1996). The carrier of this color has been tentatively identified as a red tholin-like compound (Jewitt & Luu 2001). The situation is much different in the near-infrared, where signatures of the most primitive solar system volatiles can be seen. Although many attempts have been made to detect ices on KBOs in the near-infrared, very few to date have been successful.

Barring the decades of study of Pluto, Charon and Triton (each of which could share origins with the KBOs), detections of simple organic ices on KBOs have been relatively

few. Indisputable methane ice detections have been presented for 2003 UB<sub>313</sub> and 2005 FY<sub>9</sub> (Brown et al. 2006; Barkume et al. 2005; Licandro et al. 2006). The KBO Sedna has also recently been reported to have a Triton-like spectrum, largely dominated by methane ice (Barucci et al. 2005). The following KBOs have all shown signs of water ice: (19308) 1996 TO<sub>66</sub> (Brown et al. 1999), (26375) 1999 DE<sub>9</sub> (Jewitt & Luu 2001) and (90482) Orcus (Trujillo et al. 2005). The object (50000) Quaoar has been the only KBO so far to show signs of crystalline water ice (Jewitt & Luu 2004). This finding is significant in that crystalline water ice is unstable on 10 Myr timescales. However, the presence of crystalline water ice has been seen on many other outer solar system bodies such as Charon and the giant planet moons, which argues for a common resurfacing process throughout the solar system.

In this work, we report the discovery of large amounts of crystalline water ice on 2003 EL<sub>61</sub> from observations obtained at the Gemini North telescope and Keck Observatory. The object 2003 EL<sub>61</sub> is a truly unique object in dynamical terms. It is the only known ternary or higher system in the Kuiper belt (excepting Pluto, Weaver et al. 2005), with the brighter moon's orbit reported in Brown et al. (2005) and the fainter moon reported in Brown et al. (2006). Not only is 2003 EL<sub>61</sub> a ternary system, but it is the most rapid large ( $> 100$  km) rotator in the solar system (Rabinowitz et al. 2005). The extreme rotational state of 2003 EL<sub>61</sub> combined with the measured orbit of its brighter moon yields a surprisingly large amount of information about the physical parameters of the system including limits on its shape, density and albedo (Rabinowitz et al. 2006). With the discovery of crystalline water ice on the surface of 2003 EL<sub>61</sub>, we can now place constraints on the surface fraction of water ice on the body as well as other components.

## 2. Observations

Observations of 2003 EL<sub>61</sub> were collected at the Gemini North and the Keck telescopes on Mauna Kea, Hawaii. The Gemini data were collected in queue mode on 4 separate UT dates, as detailed in Table 1. The Keck observations were collected in classical (i.e. full night) mode on UT 2005 Apr 26 and 27. Total integration times for Gemini were 4.0 hours in *K*-band, 1.3 hours in *H*-band and 1.7 hours in *J*-band using NIRI (Hodapp et al. 2003). From Keck, total integration times were 3.1 hours in a single *HK* grism setting using NIRC (Matthews & Soifer 1994). Some of the data were taken through cirrus, however, removal of the cirrus data did not affect results, so it was included in this work. A telluric standard star was taken on each night with similar airmass to the science observations. On the two photometric Gemini nights, photometry of 2003 EL<sub>61</sub> and UKIRT faint standards were taken.

### 3. Data Reduction

#### 3.1. Photometry

On the two photometric Gemini nights, synthetic aperture photometry was used to measure the broad-band colors of 2003 EL<sub>61</sub>. A large aperture of 4.7 arcseconds diameter (40 pixels) was selected due to the poor seeing (0.9 arcseconds full width at half maximum in  $H$ ). This chosen aperture encompassed the secondary which is up to 1 arcsecond away from and 3.3 magnitudes fainter than the primary. The primary has a known visible lightcurve with peak-to-peak amplitude  $0.28 \pm 0.04$  magnitudes and a period of  $3.9154 \pm 0.0002$  hours in the visible without color dependence (Rabinowitz et al. 2006). Flux measurements for  $J$ ,  $H$ , and  $K$  were made during UT 2005 Mar 02 10:34 – 11:08 and also on UT 2005 Apr 25 07:25 – 07:44. Flux measurements were compared to the Mauna Kea JHK system UKIRT standard stars FS23 and FS131 on the two respective nights (Simons & Tokunaga 2002; Tokunaga et al. 2002; Leggett 2006). Near-infrared colors were consistent between the two nights with  $J - H = -0.044 \pm 0.037$  and  $H - K = -0.111 \pm 0.048$ . These near-infrared colors were used to later scale the Gemini  $J$ ,  $H$  and  $K$  grism settings to a common relative reflectance scale. This scale was consistent with the lower resolution Keck spectrum which collected  $H$  and  $K$  using a single grism setting.

The individual  $J$ ,  $H$  and  $K$  magnitudes were all brighter on UT 2005 Apr 25 by an average of  $0.149 \pm 0.042$  magnitudes, which is consistent with the visible lightcurve measured by Rabinowitz et al. (2006). Thus, it is likely that the visible and near infrared lightcurves have the same shape and phase information, just as the  $B$ ,  $V$ ,  $R$ , and  $I$  colors do, as would be expected for a shape-dominated lightcurve. The two near infrared photometry epochs (UT 2005 Mar 02 10:51 and UT 2005 Apr 25 07:35) correspond to the lightcurve phases 0.834 and 0.016, which occur at  $-0.06$  and  $0.07$  magnitudes from the mean visible magnitude. Using the assumption that the near-infrared lightcurve and visible lightcurves match in phase and magnitude, we find the following for the mean near-infrared magnitudes for 2003 EL<sub>61</sub>:  $J = 16.518 \pm 0.020$ ,  $H = 16.561 \pm 0.031$ ,  $K = 16.672 \pm 0.037$ . These numbers are uncorrected for the solar phase angle as such values are unknown in the near infrared and likely differ from the visible. However, the solar phase angles for the two epochs are similar (0.71 degrees and 0.65 degrees, respectively), so the above magnitudes should be valid for the mean solar phase angle of 0.68 degrees. From Rabinowitz et al. (2006), we determine the mean visible magnitude to be  $V = 17.569 \pm 0.019$  at 0.68 degrees solar phase and heliocentric and geocentric distances of  $R = 51.254$  AU and  $\Delta = 50.461$  AU, corresponding to the midpoint between our near infrared photometric epochs. Thus we produce the following visible to near-infrared color:  $V - J = 1.051 \pm 0.020$ , which is consistent with solar  $V - J$  color (Jewitt & Luu 2001).

### 3.2. Spectroscopy

Both the Gemini and Keck spectral data were processed using standard near infrared techniques. First, spectra dithered along the slit were pairwise sky subtracted to remove detector bias and dark current as well as produce a first order removal of sky lines. These images were divided by a composite flat of the slit observed through the grism. The resultant image pairs were cleaned of residual bad pixels and cosmic rays. Images were rectified such that the wavelength and spatial axes were orthogonal prior to spectral extraction. Source spectra were extracted from each dither position along with adjacent sky regions. A composite residual sky spectrum was subtracted from a composite source spectrum for each night of data. Telluric G2V star spectra were put through the same processing pipeline prior to being divided into the source spectra for telluric correction to produce relative reflectance. Data from each night were then combined into a single science spectrum.

Finally, the spectral resolution of the Gemini data was reduced to match the Keck NIRC data after a search for the presence of possible narrow-band features resulted in no significant detections. The Gemini spectrum was converted to reflectance by using the measured  $J - H$  and  $H - K$  colors of 2003 EL<sub>61</sub> to scale the 3 separate  $J$ ,  $H$  and  $K$  grism settings of NIRI. Since no photometric data were collected at the Keck telescope, we scaled the single  $HK$  grism setting for Keck NIRC to the Gemini spectrum. The color-corrected Gemini spectrum in the  $H$  and  $K$  regions was consistent with the single Keck  $HK$  grism setting, so we believe that both spectra are accurate in terms of reflectance. The data from the two telescopes can be found in Figure 1. We found no significant evidence for rotational variation of spectral features in our data. There was some variation in the  $1.7 \mu\text{m}$  to  $1.8 \mu\text{m}$  range between the March and April Gemini data ( $\sim 10\%$ ) as well as the between the Gemini data and the Keck data ( $\sim 5\%$ , seen in Figure 1). We note that this region has many strong OH lines and conclude that the variations observed are likely from residual sky contamination and are not significant given the signal to noise of our data.

## 4. Pure Crystalline Water Ice Model

We produced a simple reflectance spectrum using a Hapke model and published optical constants for crystalline water ice, similar to that used by Trujillo et al. (2005). The feature at  $1.65 \mu\text{m}$ , which is obvious in our data, is found in crystalline water ice but not amorphous water ice or crystalline water ice at high temperatures (Hansen & McCord 2004). Thus, we begin our modelling of the reflectance from 2003 EL<sub>61</sub> with crystalline water ice only. The wavelength dependent absorption coefficient was drawn from Grundy & Schmitt (1998) for 30 Kelvin, and the real index of refraction from Warren (1984) was used. Isotropically

scattering grains were assumed, and an amplitude of opposition effect  $B(0) = 2.5$  was used. Many grain sizes were modeled: from  $10 \mu\text{m}$  up to 1cm diameter in size. Small grain sizes of  $25 \mu\text{m}$  to  $50 \mu\text{m}$  were universally favored to reproduce both the depth and width of the absorption. We were unable to reproduce the behavior of our spectrum shortward of  $1.2 \mu\text{m}$  with any of our models. This region is the most uncertain in the Grundy & Schmitt (1998) work, with up to factors of 2 in absorption due to fundamental limitations of the instrumental apparatus. Such large discrepancies can easily cause errors of  $\sim 5\%$  in modelled albedo, so we have ignored all wavelengths shortward of  $1.2 \mu\text{m}$  in our fits. The region beyond  $2.35 \mu\text{m}$  is also poorly fit by our models and was ignored in fitting. This wavelength region is addressed in Section 4.3.

An initial fit of the composite spectrum shows that a pure water ice model fits the major features of the spectrum and the  $J - H$  color quite well, to a few percent. However, the overall  $H - K$  color measured for 2003 EL<sub>61</sub> from the Gemini photometry, and the Keck  $HK$  grism measurement is roughly 20% lower in  $K$  flux than the pure water ice model. Regardless of the specific crystalline water ice temperature and grain sizes, if the depth of the broad absorptions are matched, the overall color of the body does not match. The pure water-ice model is pictured in Figure 1. It is clear that a component with a blue near-IR color would improve the fit, but we find no evidence for specific transitions that might indicate a particular species responsible for the blue color. We therefore considered several non-unique models which could contribute to the blue color below.

#### 4.1. The Blue Component

The water ice model residuals in Figure 1 suggests that the addition of a component with an overall blue color at near-infrared wavelengths can improve the fit substantially. Since there are no spectral signatures apparent besides the overall color, it is impossible to identify the blue component accurately. However, a survey of published infrared absorptions shows that there are at least a few common components that are blue in the near-infrared with few strong absorptions. Some of these components improve the fit significantly over the pure water ice model, although which compound is responsible for the blue near-infrared color cannot be uniquely identified from our spectral data. Nor can we place any constraint on compositions not tested; it is very likely that the true composition of 2003 EL<sub>61</sub> is quite complex and could include any, all or none of the components listed below. We believe it is useful to report on this analysis as future work may help to identify the blue component more accurately.

The three compounds that we found to improve the fit in the near-infrared are pure

hydrogen cyanide, hydrated Titan tholin and phyllosilicate clays. (Note that Titan tholins do not match the visible color of 2003 EL<sub>61</sub>, as discussed in Section 4.1.2.) Since the near-infrared colors were consistent on both photometric nights at Gemini, which probed different longitudes of the body, we believe the blue component is likely to be present across a wide surface area of the minor planet. A summary of the pure water ice model and the additional blue components are presented in Table 2 and discussion appears in following sections.

#### 4.1.1. *Hydrogen Cyanide*

Hydrogen cyanide (HCN) is one of the components we found to improve the fit significantly. A model of water ice (73%) + hydrogen cyanide (27%) improves the fit significantly as estimated by  $\chi^2$  analysis and by eye. The best-fit water ice model in this case is a 30K model with a 25  $\mu\text{m}$  grain diameter. The hydrogen cyanide model used was that of room temperature HCN (Dumas et al. 2001). No other components were added to the spectrum. Hydrogen cyanide is colorless in the visible, so HCN is consistent with the neutral  $V - J$  color measurement in this work, and the neutral  $V - I$  color reported by Rabinowitz et al. (2006).

Although the model spectrum fit is significantly improved by adding hydrogen cyanide, the lack of specific narrow features in HCN does not allow unequivocal identification in our data. Hydrogen cyanide has several weak features at 1.52  $\mu\text{m}$ , 1.68  $\mu\text{m}$ , 1.80  $\mu\text{m}$  and 2.01  $\mu\text{m}$ . The 1.52  $\mu\text{m}$ , 1.68  $\mu\text{m}$  and 2.01  $\mu\text{m}$  HCN features are very close to nearby water absorptions. These water ice absorptions change shape and depth based on the temperature and grain size assumed, so it is difficult to use any of these lines for identification of HCN. The 1.80  $\mu\text{m}$  feature is likely the most diagnostic of HCN, but it is unfortunately located in a region of the sky that is very rich in OH lines: very strong sky lines are found at 1.793  $\mu\text{m}$  and 1.799  $\mu\text{m}$ , making identification of the 1.80  $\mu\text{m}$  HCN feature impossible in our dataset and likely difficult in future datasets as well.

#### 4.1.2. *Hydrated Tholins*

The effect of adding hydrated tholins to the fit was also estimated by using the 3 tholin types discussed by Roush & Dalton (2004). The three types were the original Titan tholin manufactured by Khare et al. (1984) and measured by Cruikshank et al. (1991), as well as the Denver and Ames tholins (Roush & Dalton 2004). Addition of all three tholins improved the fit, but only the original Titan tholin, which was less hydrated than the other samples,

improved the fit at the statistically significant ( $> 3\sigma$ ) level as judged by a  $\chi^2$  analysis. The best results occurred for original tholin with 67% water ice at 30 K with 50  $\mu\text{m}$  grains + 33% original tholin. We remark that there are a wide variety of Titan tholins published, and even multiple measurements of apparently identical compounds also have resulted in discrepant laboratory spectra. Thus, we expect that it is very likely that tholin-like compounds other than those tested would also produce a significant improvement in the fit to our 2003 EL<sub>61</sub> data in the near infrared. The water + original tholin model is shown in Figure 3.

The strongest data against tholins comes from our  $V - J$  color, which is neutral in reflectance and the neutral  $V - I$  color reported by Rabinowitz et al. (2006). A common characteristic of Titan tholins is that they are red in the visible. The addition of substantial amounts (i.e. the 1/3 in our best-fit spectrum) of tholin material would certainly result in a very red surface. Thus, although the Titan tholins fit the near-infrared spectrum well, we consider them unlikely to reproduce the visible spectrum of 2003 EL<sub>61</sub>, which is colorless throughout the visible.

#### 4.1.3. *Phyllosilicate Clays*

The addition of the common Earth phyllosilicate clay kaolinite (Clark et al. 2003, W1R1Bb sample) also improves the fit somewhat. A  $\chi^2$  analysis shows that the amount of improvement falls short of formal significance, yet it was a larger improvement than for any other component tested and produced an improvement to the eye, so we include it here. The kaolinite + water ice model is shown in Figure 4. This best-fit model is composed of 81% crystalline water ice with 50  $\mu\text{m}$  grains at 30K + 19% kaolinite. The common phyllosilicate clay montmorillonite was also found to improve the fit, but to even a smaller degree than kaolinite. Data from Roush (2005) were used for montmorillonite.

Since the presence of phyllosilicate clays improves the overall fit of the spectrum, we consider these to be a possible source of the near-infrared blue color of 2003 EL<sub>61</sub>. Most montmorillonite and kaolinite clays are colorless or nearly so in the visible, so we consider these to be a reasonable component to reproduce the blue color of the near-infrared spectrum without affecting the visible color of 2003 EL<sub>61</sub>.

#### 4.1.4. *Failed Models*

We tested many other models that are somewhat blue in the near infrared as shown in Table 2 and the references therein. Several models provided no improvement at all over

the water ice model including methanol ice (Cruikshank et al. 1998), asphaltite and kerite (Moroz et al. 2004). Several models showed some improvement, but not at the formally significant level: ammonia hydrate (Dumas et al. 2001), ammonia ice (Brown & Calvin 2000), amorphous water ice (Schmitt et al. 1998, best fit with 25  $\mu\text{m}$  grains), methane ice (Grundy et al. 2002, best fit with 50  $\mu\text{m}$  grains), montmorillonite (Roush 2005) and the Ames and Denver tholin compounds (Roush & Dalton 2004). A few of these compounds deserve additional comment. Tholin compounds and montmorillonite were discussed above in Sections 4.1.2 and 4.1.3, respectively. The inclusion of asphaltite and kerite are mentioned below, in Section 4.3.

Ammonia ice and ammonia hydrate have been reported on Charon and on Quaoar (Brown & Calvin 2000; Jewitt & Luu 2004) and are of particular interest because when dissolved in water, they lower its melting point. Such compounds may make it easier to resurface a body with crystalline water ice, but we find no evidence of such compounds in our data.

Amorphous water is known to co-exist with crystalline water ice on the Galilean satellites (Hansen & McCord 2004), thus it seems possible that this could be the case for 2003 EL<sub>61</sub>, although we find no formal evidence for this in our data. It is possible that large amounts of the water ice could be amorphous (up to  $\sim 1/3$ ) without detection in our data because of the large degeneracy between crystalline water ice grain size, temperature, and amount of amorphous water ice, all of which affect the depth of the 1.65  $\mu\text{m}$  crystalline water ice feature. Much higher signal to noise spectra in the *H* band would place a stronger limit on the amount of amorphous water ice.

Although the addition of methane ice does not significantly improve our fit, because it is a known component on other solar system bodies and highly volatile, it is interesting to ask how much could be on the surface without being detected. We find that the addition of up to  $\sim 10\%$  methane ice (grainsize of 50  $\mu\text{m}$ ) results in a significant ( $> 3\sigma$ ) deviation of the model from the data in terms of  $\chi^2$  as well as by eye. We use this as a rough upper limit to the amount of methane ice that might be present on 2003 EL<sub>61</sub> because the errors in our spectra are not necessarily Gaussian, so the  $\chi^2$  statistic is not strictly appropriate in this case.

## 4.2. Neutral Absorber

We also modeled the presence of a neutral absorber. The addition of a neutral absorber of any albedo did not improve the overall fit significantly for the water ice + blue component

models, so we find no evidence for such an absorber. Our reflectance models alone cannot specifically test for the presence of highly absorbing, featureless compounds such as carbon black. The addition of such an absorber would not change the relative reflectance or the depths of the absorption bands we observe, only the overall albedo of the body. However, by using published albedo measurements, we can place some constraint on the presence of dark absorbers.

Previously, Rabinowitz et al. (2006) placed constraints on the albedo of 2003 EL<sub>61</sub> from lightcurve and binary orbit measurements. The spheroidal and ellipsoidal models place the *V*-band albedo in the  $0.6 < p_V < 0.8$  range. Such albedo measurements are consistent with our models, which include no dark or neutral materials. Since the  $V - J$  color is roughly solar, then the *J* albedo and *V* albedo are roughly equal. Using this information, we find that all of the two-component models in Figures 2–4 fall within  $0.75 < p_V < 0.90$ , showing a reasonable consistency between the dynamical spin models and our icy near-infrared reflectance models. Thus, we expect the true surface fractions of ices on 2003 EL<sub>61</sub> to be very close to the reflectance model fractions presented here, with very little low albedo material present on the surface.

### 4.3. The 2.35 $\mu\text{m}$ Turndown

We note that there is a clear drop in the spectrum of 2003 EL<sub>61</sub> beyond 2.35  $\mu\text{m}$  compared to the crystalline water ice model as well as the water ice + blue component models. This turndown is observed in both the Keck spectrum and the Gemini spectrum. The feature appears to start at about 2.35  $\mu\text{m}$  and continues until atmospheric sky noise overcomes the object signal at  $\sim 2.45 \mu\text{m}$ . Thus, it appears that the central wavelength of this absorption is at or beyond 2.45  $\mu\text{m}$ . Such an absorption has been seen in other solar system bodies. High signal to noise observations of Charon have shown a similar feature, but the carrier was never identified (Brown & Calvin 2000). A similar absorption has been reported on Pheobe, and has been attributed to a cyanide combination, possibly potassium cyanide or cyanide trihydrate (Clark et al. 2005b). Such absorption has also been reported by Clark et al. (2005a) for Iapetus, Dione, and the F-ring. Judging from Clark et al. (2005b), the reflectance of 2003 EL<sub>61</sub> appears to be most consistent with copper potassium cyanide in this region, as it is broad ( $\sim 0.1 \mu\text{m}$ ) and in the correct location. We did not specifically model this compound in more detail because we were unable to find data on its absorption shortward of 1.8  $\mu\text{m}$  in any available literature or chemical database.

Although potassium cyanide and cyanide trihydrate may be responsible for the observed turndown, other inorganic cyanide salts ( $-\text{C}\equiv\text{N}$ ) are not a good match. Nickel cyanide,

cadmium cyanide and zinc cyanide all produce very narrow transitions (widths about 0.03  $\mu\text{m}$ ) shortward of 2.36  $\mu\text{m}$  (Clark et al. 2003). Such narrow transitions are inconsistent with the 2.35  $\mu\text{m}$  turndown, which appears to extend longward of 2.45  $\mu\text{m}$ . It would be interesting to test organic nitrile compounds ( $-\text{C}-\text{N}\equiv\text{C}$ ) as they share the  $\text{C}\equiv\text{N}$  triple bond with inorganic cyanide salts, but we were unable to find suitable spectral information for these components.

The addition of bitumens such as kerite, asphaltite or wurtzilite, which have a drop at 2.3  $\mu\text{m}$  could also explain the 2.35  $\mu\text{m}$  turndown (Moroz et al. 1998). These compounds are in general fairly red, so although their inclusion may improve the fit beyond 2.3  $\mu\text{m}$ , they would likely make the overall color of the model spectrum deviate from our measured reflectance. We examined the use of both powdered kerite and asphaltite (Moroz et al. 2004), but neither appeared to improve the overall fit significantly due to the steep red slope seen at wavelengths shorter than 1.5  $\mu\text{m}$ .

## 5. Discussion

The basic result of our observations is that the spectrum of 2003 EL<sub>61</sub> is consistent with a model with roughly 2/3 to 4/5 pure crystalline water ice combined with 1/3 to 1/5 pure blue material. The best candidates for the blue material we could find are pure hydrogen cyanide ice or possibly phyllosilicate clays, although this identification is not unique. Likely there are many possible materials that could fit the near-infrared color of 2003 EL<sub>61</sub>, of which only a fraction have lab spectra available. No neutral absorbers are needed in appreciable amounts to model the relative reflectance of the body. The only feature noted in the near infrared spectrum besides that of crystalline water ice and the basic blue color is the turndown beyond 2.3  $\mu\text{m}$  which is consistent with copper potassium cyanide. Laboratory data on cyanide compounds is sparse, so it is likely that other cyanide compounds could produce such behavior.

The presence of crystalline water ice has been widely reported for many outer solar system bodies such as the satellites of the major planets, Charon and most recently Quaoar. As noted by Jewitt & Luu (2004) for (50000) Quaoar, the presence of crystalline water ice is considered problematic in the Kuiper belt because, in general, lower energy amorphous ice is favored in cold environments. It is easy to imagine that crystalline water ice may have been prevalent in the solar system due to heating events in the early solar nebula. In such a case, it is possible that crystalline water ice can be incorporated into bodies at low temperatures ( $< 100\text{K}$ ) if the deposition flux of water molecules is low (Kouchi et al. 1994). However, the disruptive action of cosmic ray and solar flux bombardment on the outer surfaces of icy

bodies is expected to rearrange crystalline water ice to amorphous in the outer solar system (Hansen & McCord 2004).

Both solar flux and cosmic ray bombardment can cause extensive radiation damage to the outer surface layers of KBOs. Estimating the time scale of such radiation damage is very difficult due to the sparse amount of data available about energetic particles in the solar system, which comes primarily from spacecraft. In addition, assumptions about the timescale for density changes in the local interstellar medium must be made which directly affects all estimates of the extent of the heliosphere, which is a key component of radiation damage models. Our near-infrared reflectance spectra observations probe the first  $\sim 1 \mu\text{m}$  of the KBO surface. The solar system irradiation model of Cooper et al. (2003) suggests that disruptive amounts of energy (of order  $\sim 100 \text{ eV}$  per 16 amu) can be delivered to  $\sim 1 \mu\text{m}$  depths by Galactic Cosmic Rays in the solar system lifetime throughout the heliosphere. Timescales several orders of magnitude shorter may be plausible both closer to and farther from the sun than the  $\sim 40 \text{ AU}$  region of the Kuiper Belt. As many of these KBOs have been at their present location for  $10^9$  years even in extreme dynamical models (Gomes et al. 2005), it appears that a solar system wide model for surface renewal is likely needed to explain the presence of crystalline water ice.

Hydrogen cyanide, one of the species that can explain the blue near infrared color of 2003 EL<sub>61</sub>, is also photolysed rapidly in the outer solar system environment. Whether alone or frozen in solution with water ice, hydrogen cyanide is destroyed after deposition of about 100 eV per molecule by both irradiation and photolysis (Gerakines et al. 2005). Thus if HCN is to be considered as a source of the blue material on 2003 EL<sub>61</sub>, it has the same stability problems as crystalline water ice. The phyllosilicate clays, another possible infrared blue material, do not share this sensitivity to radiation damage.

## 6. Summary

Using the Gemini and Keck telescopes, we have measured the near-infrared reflectance spectrum of 2003 EL<sub>61</sub> on a global scale. We find the following:

- The presence of crystalline water ice dominates the spectrum. Best fit models require between 2/3 and 4/5 of the reflectance to be attributed to pure crystalline water ice.
- As for other outer solar system bodies, crystalline water ice is unstable on solar system timescales, suggesting some kind of global surface renewal process.
- The addition of a second component that is blue in the near-infrared dramatically

increases the goodness of fit and is responsible for 1/3 to 1/4 of the reflectance. The most likely carriers for this component are hydrogen cyanide or phyllosilicate clays, although this identification is not unique. Although hydrated titan tholins do improve the near-infrared fit, they are inconsistent with the neutral visible color observed for 2003 EL<sub>61</sub>.

- The presence of inorganic cyanide salts such as copper potassium cyanide may explain the observed absorption beyond 2.3  $\mu\text{m}$ , as has been postulated for Pheobe and other Saturnian bodies (Clark et al. 2005b).
- There is likely to be very little low albedo material on the surface of 2003 EL<sub>61</sub> as our pure ice model albedos are consistent with published lightcurve/orbit dynamical constraints (Rabinowitz et al. 2006). Thus, the fractions described for reflectance are similar to the global surface coverage for the ices described. This surface coverage can only be estimated to the  $\sim 1 \mu\text{m}$  depth, our characteristic wavelength of observation.
- No more than  $\sim 10\%$  of the surface of 2003 EL<sub>61</sub> could be covered with methane ice without detection.
- The near-infrared photometric differences between the two epochs we observed are consistent with the previously published visible lightcurve of 2003 EL<sub>61</sub>, which is attributed to pronounced global rotational distortion of the body. The ubiquity of these variations from 0.4 – 2.5  $\mu\text{m}$  adds more evidence to the conclusion that the extreme lightcurve of 2003 EL<sub>61</sub> is due to shape only.

We thank the Gemini science staff who scheduled our program, operated the telescope and collected the queue mode data: Tracy Beck, Julia Bodnarik, Simon Chan, Avi Fhima, Rachael Johnson, Inger Jørgensen, Andrew Stephens, Kevin Volk, and Dolores Walther. We thank the observing assistants and support astronomers at the W. M. Keck Observatory who helped with this project: Marc Kassis, Chuck Sorenson and Steven Magee. This work was based on observations obtained at the Gemini Observatory, which is operated by the Association of Universities for Research in Astronomy, Inc., under a cooperative agreement with the NSF on behalf of the Gemini partnership: the National Science Foundation (United States), the Particle Physics and Astronomy Research Council (United Kingdom), the National Research Council (Canada), CONICYT (Chile), the Australian Research Council (Australia), CNPq (Brazil) and CONICET (Argentina). Observations were collected under Gemini program IDs GN-2004B-Q-56 and GN-2005A-Q-45. Some of the data presented herein were obtained at the W. M. Keck Observatory, which is operated as a scientific partnership among the California Institute of Technology, the University of California, and the

National Aeronautics and Space Administration. The Observatory was made possible by the generous financial support of the W. M. Keck Foundation.

## REFERENCES

Barkume, K. M., Brown, M. E., & Schaller, E. L. 2005, AAS/Division for Planetary Sciences Meeting Abstracts, 37

Barucci, M. A., Cruikshank, D. P., Dotto, E., Merlin, F., Poulet, F., Dalle Ore, C., Fornasier, S., & de Bergh, C. 2005, *A&A*, 439, L1

Brown, M. E., et al. 2005, *ApJ*, 632, L45

Brown, M. E., & Calvin, W. M. 2000, *Science*, 287, 107

Brown, M. E., Trujillo, C. A., & Rabinowitz, D. L. 2006, Submitted to *ApJ*

Brown, M. E., et al. 2006, submitted to *ApJ*

Brown, R. H., Cruikshank, D. P., & Pendleton, Y. 1999, *ApJ*, 519, L101

Clark, R. N., et al. 2005a, AGU Fall Meeting Abstracts, A2

Clark, R. N., et al. 2005b, *Nature*, 435, 66

Clark, R. N., Swayze, G. A., Wise, R., Livo, K. E., Hoefen, T. M., Kokaly, R. F., & Sutley, S. J. 2003, U.S. Geological Survey, Open File Report 03-395

Cooper, J. F., Christian, E. R., Richardson, J. D., & Wang, C. 2003, *Earth Moon and Planets*, 92, 261

Cruikshank, D. P., Allamandola, L. J., Hartmann, W. K., Tholen, D. J., Brown, R. H., Matthews, C. N., & Bell, J. F. 1991, *Icarus*, 94, 345

Cruikshank, D. P., et al. 1998, *Icarus*, 135, 389

Dumas, C., Terrile, R. J., Brown, R. H., Schneider, G., & Smith, B. A. 2001, *AJ*, 121, 1163

Gerakines, P. A., Bray, J. J., Davis, A., & Richey, C. R. 2005, *ApJ*, 620, 1140

Gomes, R., Levison, H. F., Tsiganis, K., & Morbidelli, A. 2005, *Nature*, 435, 466

Grundy, W. M., & Schmitt, B. 1998, *J. Geophys. Res.*, 103, 25809

Grundy, W. M., Schmitt, B., & Quirico, E. 2002, *Icarus*, 155, 486

Hansen, G. B., & McCord, T. B. 2004, *Journal of Geophysical Research (Planets)*, 109, 1012

Hodapp, K. W., et al. 2003, *PASP*, 115, 1388

Jewitt, D. C., & Luu, J. 2004, *Nature*, 432, 731

Jewitt, D. C., & Luu, J. X. 2001, *AJ*, 122, 2099

Khare, B. N., Sagan, C., Arakawa, E. T., Suits, F., Callcott, T. A., & Williams, M. W. 1984, *Icarus*, 60, 127

Kouchi, A., Yamamoto, T., Kozasa, T., Kuroda, T., & Greenberg, J. M. 1994, *A&A*, 290, 1009

Leggett, S. 2006, In preparation

Licandro, J., Pinilla-Alonso, N., Pedani, M., Oliva, E., Tozzi, G. P., & Grundy, W. M. 2006, *A&A*, 445, L35

Luu, J., & Jewitt, D. 1996, *AJ*, 112, 2310

Matthews, K., & Soifer, B. T. 1994, in *Infrared Astronomy with Arrays: the Next Generation*, 239

Moroz, L., Baratta, G., Strazzulla, G., Starukhina, L., Dotto, E., Barucci, M. A., Arnold, G., & Distefano, E. 2004, *Icarus*, 170, 214

Moroz, L. V., Arnold, G., Korochantsev, A. V., & Wasch, R. 1998, *Icarus*, 134, 253

Rabinowitz, D., Tourtellotte, S., Brown, M., & Trujillo, C. 2005, *AAS/Division for Planetary Sciences Meeting Abstracts*, 37,

Rabinowitz, D. L., Barkume, K., Brown, M. E., Roe, H., Schwartz, M., Tourtellotte, S., & Trujillo, C. A. 2006, to appear in *ApJ*

Roush, T. L. 2005, *Icarus*, 179, 259

Roush, T. L., & Dalton, J. B. 2004, *Icarus*, 168, 158

Schmitt, B., Quirico, E., Trotta, F., & Grundy, W. M. 1998, in *ASSL Vol. 227: Solar System Ices*, 199

Simons, D. A., & Tokunaga, A. 2002, *PASP*, 114, 169

Tokunaga, A. T., Simons, D. A., & Vacca, W. D. 2002, PASP, 114, 180

Trujillo, C. A., Brown, M. E., Rabinowitz, D. L., & Geballe, T. R. 2005, ApJ, 627, 1057

Warren, S. G. 1984, Appl. Opt., 23, 1206

Weaver, H. A., et al. 2005, IAU Circ., 8625, 1

Table 1. Gemini Observations of 2003 EL<sub>61</sub>

UT date	UT time	Grating	Airmass	Exposure Time [min]	Sky
2005 Jan 27	13:36 – 14:46	<i>K</i> -grism	1.098 – 1.013	65	Thin Cirrus
2005 Jan 27	15:51 – 16:18	<i>K</i> -grism	1.008 – 1.024	25	Photometric
2005 Mar 02	10:34 – 10:40	<i>J</i> photometry	1.239 – 1.218	4	Photometric
2005 Mar 02	10:40 – 10:47	<i>H</i> photometry	1.215 – 1.196	4	Photometric
2005 Mar 02	10:47 – 11:08	<i>K</i> photometry	1.193 – 1.135	4	Photometric
2005 Mar 02	11:25 – 12:18	<i>K</i> -grism	1.091 – 1.024	50	Photometric
2005 Mar 02	12:24 – 13:17	<i>H</i> -grism	1.015 – 1.000	50	Photometric
2005 Mar 02	13:21 – 13:53	<i>J</i> -grism	1.002 – 1.015	30	Photometric
2005 Apr 25	07:25 – 07:31	<i>J</i> photometry	1.153 – 1.138	4	Photometric
2005 Apr 25	07:32 – 07:38	<i>H</i> photometry	1.136 – 1.122	4	Photometric
2005 Apr 25	07:38 – 07:44	<i>K</i> photometry	1.120 – 1.107	4	Photometric
2005 Apr 25	08:04 – 08:57	<i>K</i> -grism	1.065 – 1.013	50	Photometric
2005 Apr 25	11:29 – 12:09	<i>J</i> -grism	1.133 – 1.239	25	Photometric
2005 Apr 25	12:10 – 12:41	<i>H</i> -grism	1.260 – 1.381	30	Photometric
2005 May 31	08:56 – 09:59	<i>K</i> -grism	1.111 – 1.294	50	Cirrus
2005 May 31	10:00 – 11:01	<i>J</i> -grism	1.320 – 1.688	45	Cirrus



Table 2. Spectral Models of 2003 EL<sub>61</sub>

Water Grain Size [μm]	Water Ice Fraction	Secondary Component	Secondary Fraction	Improvement over water ice model	Visible Color
25	100%	50 μm Water ice <sup>a</sup>	0%	N/A	Neutral
25	73%	HCN <sup>b</sup>	27%	Significant	Neutral
50	67%	Original tholin <sup>c</sup>	33%	Significant	Red
50	81%	Kaolinite <sup>d</sup>	19%	Borderline	Neutral
		Ammonia hydrate <sup>b</sup>		Insignificant	Neutral
		Ammonia ice <sup>e</sup>		Insignificant	Neutral
		25 μm Amorphous Water <sup>f</sup>		Insignificant	Neutral
		50 μm Methane ice <sup>g</sup>		Insignificant	Neutral
		Montmorillonite <sup>h</sup>		Insignificant	Neutral
		Ames tholin <sup>c</sup>		Insignificant	Red
		Denver tholin <sup>c</sup>		Insignificant	Red
		Methanol ice <sup>i</sup>		None	Neutral
		Asphaltite <sup>j</sup>		None	Red
		Kerite <sup>j</sup>		None	Red

<sup>a</sup>Grundy & Schmitt (1998) and Warren (1984)

<sup>b</sup>Dumas et al. (2001)

<sup>c</sup>Roush & Dalton (2004)

<sup>d</sup>Clark et al. (2003)

<sup>e</sup>Brown & Calvin (2000)

<sup>f</sup>Schmitt et al. (1998)

<sup>g</sup>Grundy et al. (2002)

<sup>h</sup>Roush (2005)

<sup>i</sup>Cruikshank et al. (1998)

<sup>j</sup>Moroz et al. (2004)

Note. — Compounds that are neutral or nearly so in the visible are favored because of the neutral visible color of 2003 EL<sub>61</sub>. See text for complete discussion.

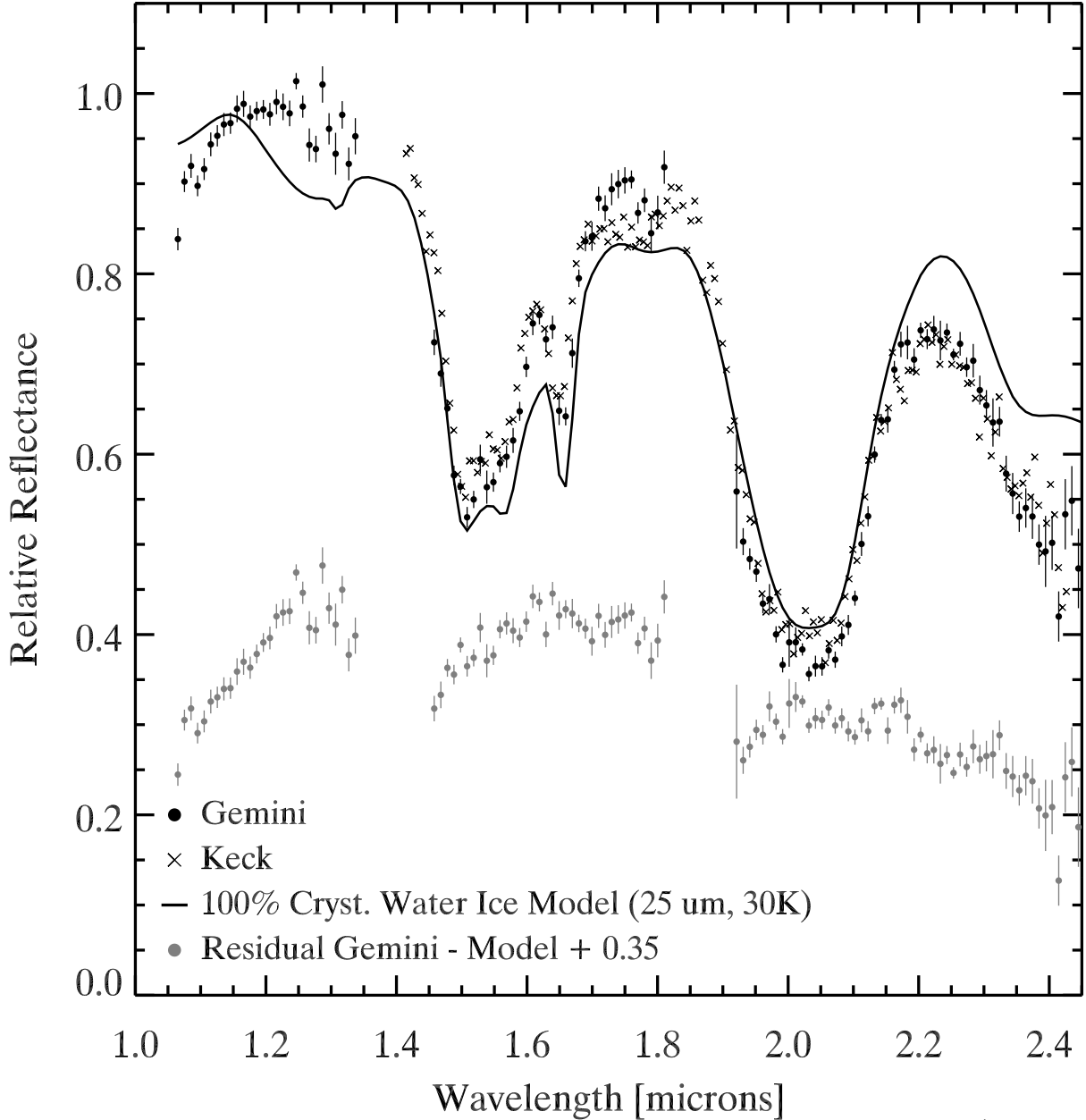


Fig. 1.— Relative reflectance spectrum of 2003 EL<sub>61</sub> from Gemini and Keck (black filled circles and x's) normalized to the model. Overplotted is our best fit 100% pure crystalline water ice model at its true geometric albedo. The spectrum - model residuals (gray filled circles) illustrate that an additional blue component is needed to reproduce the near-infrared colors of 2003 EL<sub>61</sub>, particularly in the *H* to *K* region. See text for full details of the model.

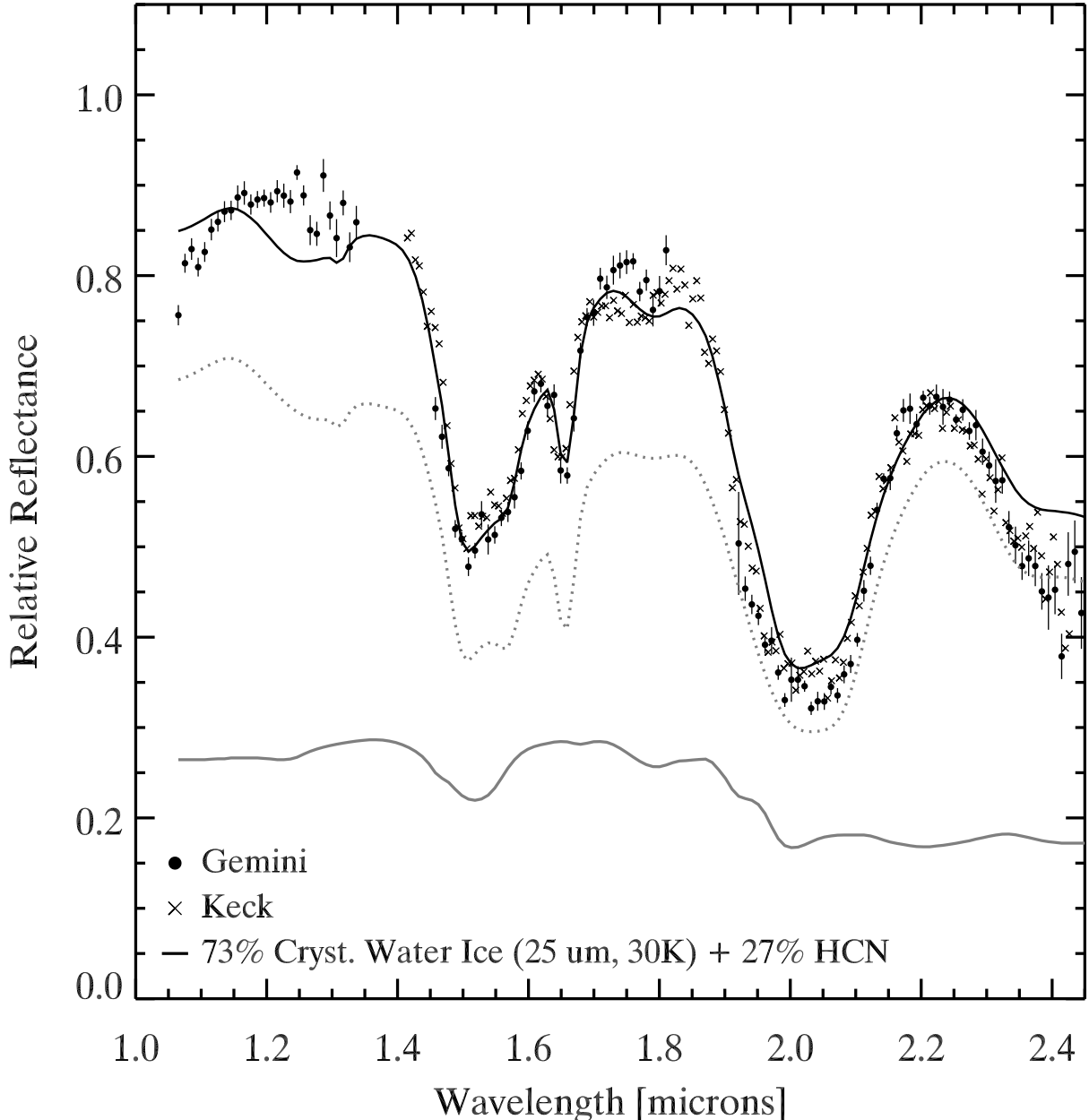


Fig. 2.— Relative reflectance spectrum of 2003 EL<sub>61</sub> from Gemini and Keck (black filled circles and x's) normalized to the model. Overplotted is our best fit pure crystalline water ice model with cyanide (HCN) at its true geometric albedo. The individual water ice and HCN components (shifted vertically by 0.1 for clarity) appear as a dotted line and solid gray line respectively. See text for full details of the models.

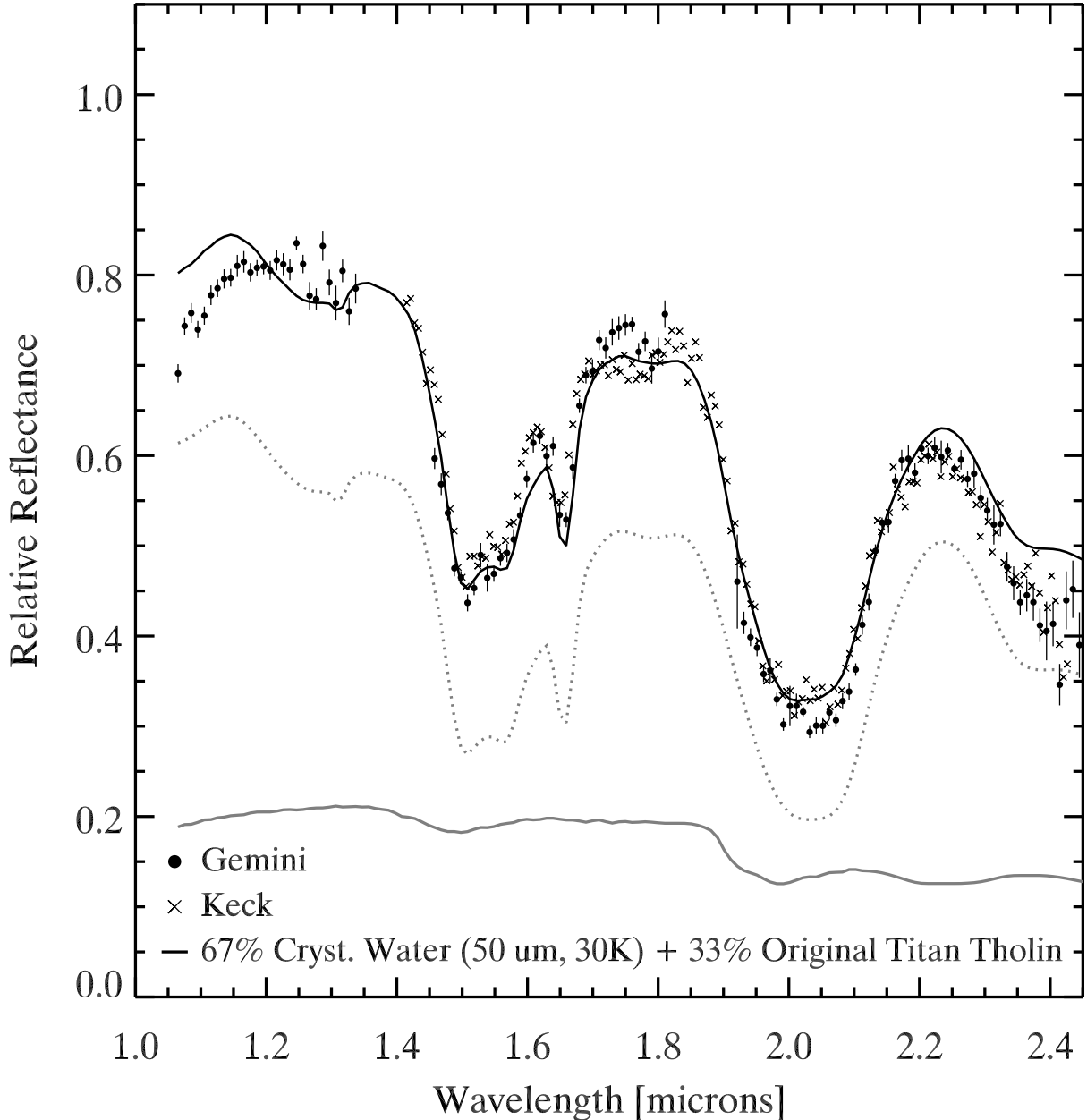


Fig. 3.— Relative reflectance spectrum of 2003 EL<sub>61</sub> from Gemini and Keck (black filled circles and x's) normalized to the model. Overplotted is our best fit 100% pure crystalline water ice model with hydrated tholin at its true geometric albedo. The individual water ice and hydrated tholin components appear as a dotted line and a solid gray line respectively. See text for full details of the models. Note that although tholins improve the fit in the near infrared, such large amounts are ruled out by the neutral visible color of 2003 EL<sub>61</sub>.

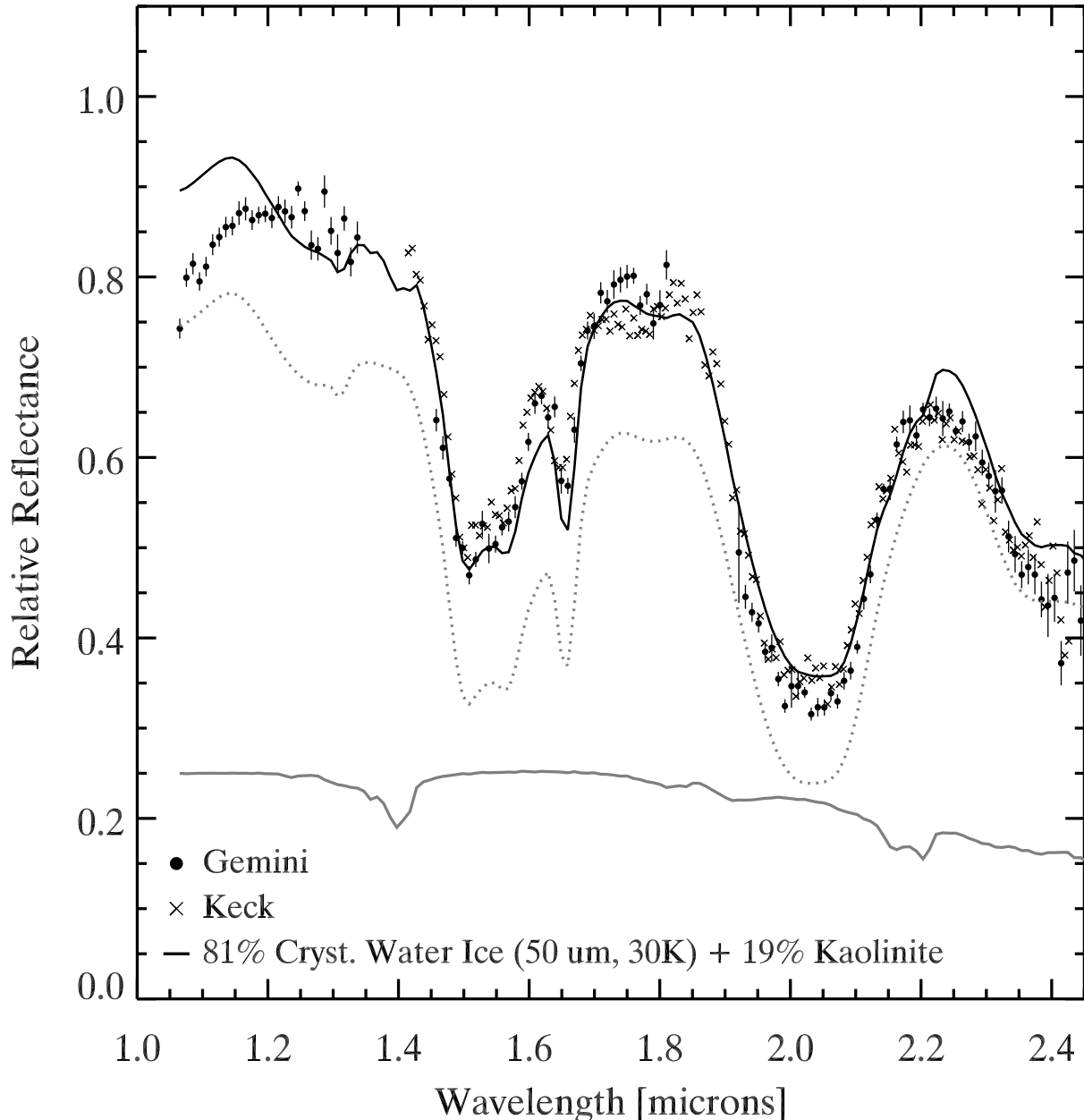


Fig. 4.— Relative reflectance spectrum of 2003 EL<sub>61</sub> from Gemini and Keck (black filled circles and x's) normalized to the model. Overplotted is our best fit 100% pure crystalline water ice model with kaolinite clay at its true geometric albedo. The dotted line is the water ice component and the solid gray line is the spectrum of kaolinite alone, shifted upwards by 0.1 for clarity. See text for full details of the models.